MATERIALS SCIENCE

Capillarity-induced folds fuel extreme shape changes in thin wicked membranes

Paul Grandgeorge,[1] Natacha Krins,[2] Aurélie Hourlier-Fargette,[1,3] Christel Laberty-Robert,[2] Sébastien Neukirch,[1] Arnaud Antkowiak[1,4]*

Soft deformable materials are needed for applications such as stretchable electronics, smart textiles, or soft biomedical devices. However, the design of a durable, cost-effective, or biologically compatible version of such a material remains challenging. Living animal cells routinely cope with extreme deformations by unfolding preformed membrane reservoirs available in the form of microvilli or membrane folds. We synthetically mimicked this behavior by creating nanofibrous liquid-infused tissues that spontaneously form similar reservoirs through capillarity-induced folding. By understanding the physics of membrane buckling within the liquid film, we developed proof-of-concept conformable chemical surface treatments and stretchable basic electronic circuits.

Geometry is behind the curious mechanical behavior of the capture silk spun by ecribellate spiders: Whether stretched or compressed, this fiber remains straight while seemingly adjusting its length, as if telescopic. In reality, the pulling force caused by surface tension allows coiling, spooling, and packing of excess fiber within the glue droplets decorating the thread. These fiber reservoirs can be recruited on demand and give the thread an apparent extreme stretchability of +10,000% (*1*). Another example are cells that display a particular ability to cope with stretch. Macrophages extend their surface area by a factor of 5 to engulf large microbes or cellular debris (*2*), patroling T lymphocytes stretch by 40% to squeeze into the microvasculature (*3*), hundreds of micrometer-sized neuronal projections extrude from 10-μm-wide neurons (*4*, *5*), and the osmotic swelling of fibroblasts leads to a 70% increase in area (*6*). Such an extreme deformability is all the more spectacular given that the lytic stretching level at which the plasma membrane ruptures is about 4% (*4*, *7*). Why do these cells not burst under stress? Cells store excess membrane in the form of folds and microvilli (*8*, *9*) that can be recruited and deployed on demand. These local geometrical ruffles do not alter the global shape of the cell, because cellular tension is preserved with the pulling action of the underlying cortical actin layer (*10*). The considerable deformations that biological materials undergo could inspire a new generation of synthetic stretchable materials, which are in demand for emerging technologies such as stretchable electronics (*11*), flexible batteries (*12*), smart textiles (*13*), biomedical devices, tissue engineering, and soft robotics (*14*, *15*).

Our technique for making synthetic fabrics with high stretchability takes advantage of spontaneously formed membrane folds and ruffles. Figure 1 illustrates the key steps in designing such an extensible tissue. We first manufacture, using an electrospinning technique, a light and free-standing nonwoven fabric made of poly(vinylidene fluoride-co-hexafluoropropylene) (PVDF-HFP; Fig. 1) (*16*). Without further treatment, this membrane would show early signs of damage above a few percent of extension and would rupture at 30% area extension. We therefore infuse the fibrous membrane with a wetting liquid, so as to mimic the pulling action of the cortical actin layer with surface tension. The membrane becomes tight while seemingly adjusting its surface, storing any excess membrane into a venation network (visible in Fig. 1 and movie S1), thus remaining globally flat. These veins are made of membrane ruffles and furrows that can be unfolded as required, fueling any imposed shape change to the membrane. By buffering excess membrane and mediating stretching, these veins play the same role as the membrane reservoirs in living cells, and we therefore refer to these structures as reservoirs. The unfolding process is reversible; the membrane reservoirs, after being smoothed out upon extension, spontaneously reform upon compression.

To elucidate the mechanics of membrane reservoir formation, we investigated the inner conformation of the membrane within the liquid film. Figure 2 presents microscopic views revealing that the flat membrane portions are actually lightly wrinkled with a wavelength λ, whereas

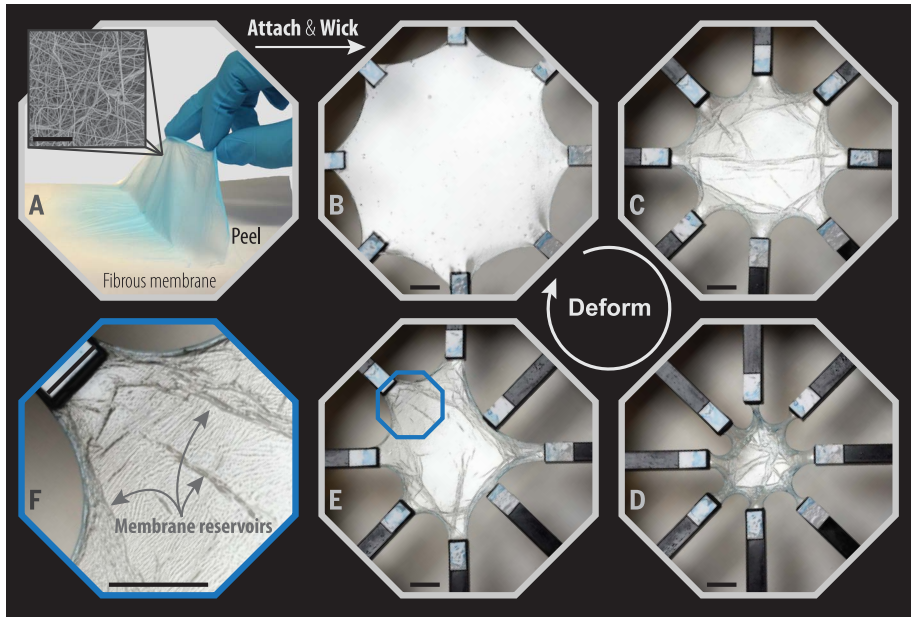

Fig. 1. Design of the ultrastretchable wicked membrane. (**A**) A thin fibrous membrane (electrospun PVDF-HFP membrane dyed blue) and the corresponding scanning electron microscope micrograph. The membrane has a typical thickness of a few micrometers; the fibers composing it have diameters around 300 nm. Scale bar, 50 μm. (**B**) The membrane is attached to eight translational supports and wicked with 3 cSt silicone oil. (**C** to **E**) The eight supports are brought together, but the wicked membrane remains globally flat by locally storing excess membrane in apparent veins. (**F**) A closer view of these veins, or membrane reservoirs, which buffer the imposed deformations on the wicked membrane. Scale bars in (B) to (F), 1 cm.

[1]Sorbonne Université, CNRS, Institut Jean le Rond ∂'Alembert, F-75005 Paris, France. [2]Sorbonne Université, CNRS, Laboratoire de Chimie de la Matière Condensée de Paris, F-75005 Paris, France. [3]PSL Research University, CNRS, École Normale Supérieure, Département de Physique, F-75005 Paris, France. [4]Saint-Gobain, CNRS, Surface du Verre et Interfaces, F-93303 Aubervilliers, France.
***Corresponding author. Email: arnaud.antkowiak@upmc.fr**

the veins are made up of a stack of folds and both the lightly wrinkled and stacked regions are sheathed between slightly rippled liquid interfaces (movie S2). We first focus on the emergence of the lightly wrinkled pattern (Fig. 2B, panel b). Wrinkling is a trademark of thin elastic sheets, and it develops spontaneously in a variety of contexts: pinched skin, shriveling fruits (*17*), brain sulci (*18*), hanging curtains (*19*), or, more generally, thin sheets under tension (*20*). This elastic instability occurs whenever a compressed slender structure is bound to a substrate resisting deformation. The emerging wavelength λ of this particular form of buckling therefore results from a trade-off between the deformation of the membrane and that of the substrate in order to minimize global energy. Here, the substrate role is played by the liquid film interfaces, which can be seen as soft capillary walls confining the membrane. Experiments revealed that the wavelength λ is neither particularly sensitive to the interfacial tension γ, nor to the fibrous membrane thickness t_0, but scales linearly with the liquid film thickness h, which is measured by means of colorimetry (Fig. 2D and figs. S1 and S2) (*16*).

We developed a simple model in which a periodic sinusoidal membrane of bending stiffness B per unit depth interacts with a liquid film, exposing two free interfaces of surface tension γ (Fig. 2C and figs. S8 and S9) (*16*). This model ignores the effects of gravity on wavelength, but gravity only plays an important role in the orientation of the wrinkling pattern (*16*) (figs. S16 to S20). Under the constraint of constant liquid film volume and imposed compression ε, we minimize the total energy of the system, consisting of the membrane elastic energy $E_{el} = \frac{1}{2}B\int\kappa^2\,ds$ and the surface energy $E_\gamma = 2\gamma S$, where κ and S respectively denote the local membrane curvature and the exposed surface of the liquid film per unit depth (*16*). The model reveals h/L_{ec} as a relevant parameter of the system, where $L_{ec} = (B/\gamma)^{1/2}$ is the elastocapillary length (*21*). The limit $h/L_{ec} << 1$ typically corresponds to everyday-life soaked fibrous membranes (e.g., wet paper or cloth) that sag or buckle globally when compressed, irrespective of any surface tension effects (Fig. 2C). Conversely, our experiment is characterized by values of $h/L_{ec} >> 1$ for which the microstructure differs markedly from that of a common wet fabric: Interface energies can no longer be neglected, and the membrane now buckles under capillary confinement (Fig. 2C). In this regime, the ratio of surface energy to elastic energy scales as $E_\gamma/E_{el} \sim (h/L_{ec})^2 >> 1$; that is, any deformation of the liquid surface introduces a strong energetic penalty, which means that in-film wrinkling is a low-energy configuration. This phenomenon is therefore reminiscent of buckling under rigid confinement, for which the wavelength λ also scales linearly with the confinement gap h for a given compression ε (*22*), and this behavior is recovered by our model (Fig. 2D, inset, and fig. S10). In contrast to classic buckling under confinement (*22*), the experimentally measured wavelengths λ prove to be insensitive to compression. This

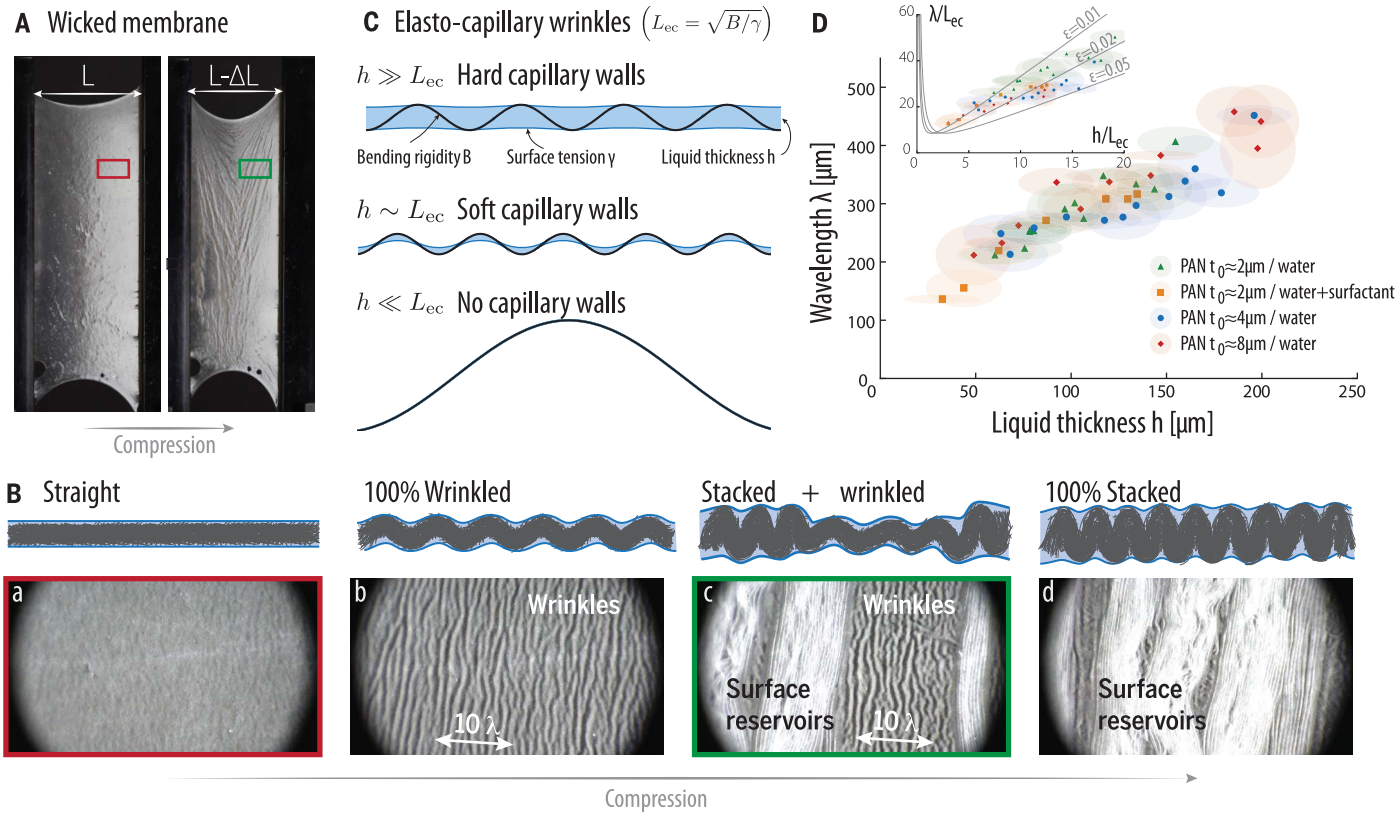

Fig. 2. Mechanics of the wicked membrane: Capillary-driven wrinkling and stacking. (**A**) Polyacrylonitrile (PAN) membrane wicked with water and attached to two straight mobile edges. Upon small compression, the wicked membrane exhibits a clear wrinkling pattern (L = 4 cm). (**B**) Close-up on the wicked membrane throughout compression. At its extended state, the wicked membrane is smooth (a) and a small compression generates a wrinkled surface of wavelength λ (b). Further compression then leads to a two-phase texture (c). One phase corresponds to the wrinkled texture (wavelength λ) and the other to a closely packed stack of folds, which gradually expands throughout compression. The whole membrane is packed in this stack of folds at the end of compression (d). Scale: 10λ = 3.1 mm. (**C**) Physical interpretation of the early wrinkling of the membrane inside the liquid film. Depending on the ratio of liquid film thickness to elasto-capillary length, h/L_{ec}, three different buckling scenarios emerge. (**D**) Experimental wavelength λ of the wrinkles observed at an early compression stage of the wicked PAN membrane as a function of the liquid film thickness h for different membrane thicknesses t_0 and wicking liquids. The inset provides the data normalized by the elasto-capillary length L_{ec} (*16*).

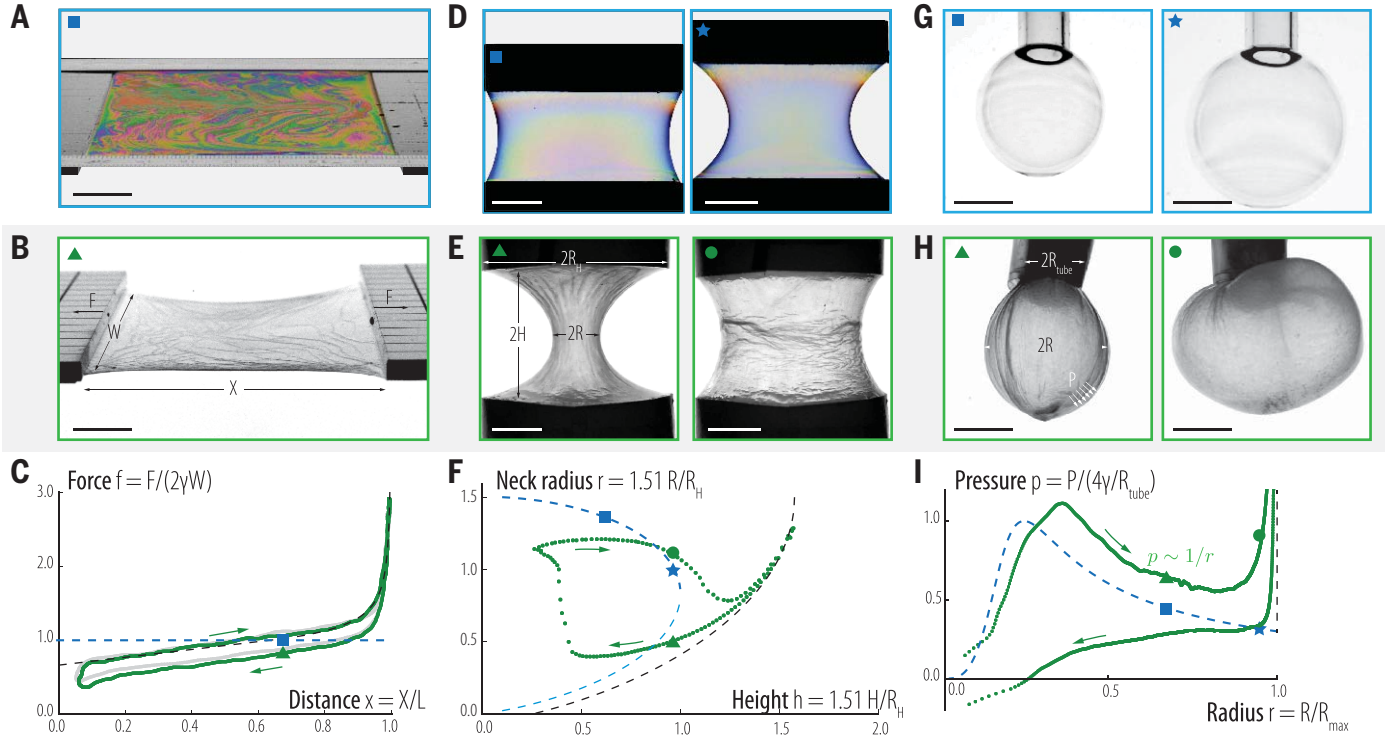

Fig. 3. Forms and forces for capillary-folded wicked membranes. (**A**) Soap liquid film on a frame. (**B**) Planar wicked membrane attached to two mobile supports. (**C**) The green curve corresponds to the force measurements during the first compression/extension cycle of a planar PVDF-HFP wicked membrane whereas the gray curve was obtained after imposing 100,000 compression/extension cycles on the membrane. The blue dashed line shows the force prediction on a planar soap film on a rigid frame; the black dashed line corresponds to the theoretical prediction with inextensibility constraint (*16*). (**D**) Soap liquid catenoid between two parallel circular rings. (**E**) Two states of the catenoid shape adopted by a wicked membrane attached to two parallel circular rings. (**F**) Neck radius of the catenoid versus distance between the two rings. The green points represent the experimental observation for a wicked membrane. The blue dashed line shows the soap liquid solution for the catenoid and the black dashed line shows the solution for a catenoid with inextensibility constraint (*16*). (**G**) Soap bubble. (**H**) Bubble generated by inflating a wicked membrane at two different inflating stages. (**I**) Pressure versus radius diagram. Here, the radius of a bubble is defined as $R = [(3/4\pi)V]^{1/3}$, where V is the volume of injected air. The blue dashed line represents the theoretical pressure for a soap bubble being inflated through a tube of radius R_{tube} (Laplace's law). The green points correspond to the pressure measurements of the wicked membrane. Scale bars, 1 cm.

behavior, not captured by the model, coincides with the emergence of a second phase in mechanical equilibrium with the first wrinkled phase. This second phase, corresponding to the membrane reservoir, consists of tightly stacked folds and is therefore characterized by a high membrane storage capacity (Fig. 2B). The coexistence between these phases allows continuous transfer of material from one phase to another and ensures the effectiveness of the wicked membrane as a stretchable material.

We next subjected wicked membranes to three different elementary deformations corresponding to the stretching of planar, cylindrically shaped, and spherically shaped membranes (movies S3 to S5, respectively). The equilibrium shape adopted by the wicked membrane in each configuration strongly resembles that of a liquid film under the same conditions: planar film (Fig. 3B), catenoid (Fig. 3E and fig. S5), and bubble (Fig. 3H and fig. S6). Once again, this behavior is made apparent by realizing that in the limit $h/L_{ec} >> 1$, the energy of the wicked membrane is dominated by its capillary contribution; the equilibrium shapes therefore essentially correspond to minimal surfaces. Although they differ strongly in longevity, fabrication methods, and internal structure, the wicked membranes and liquid films therefore present interesting similarities. Upon closer inspection, however, the shapes of the membranes appear to differ from their liquid counterparts in some respects. For example, a planar wicked membrane attached on only two straight edges adopts a stable shape (Fig. 3, A to C), whereas a liquid film in the same configuration would burst. To understand this stabilization mechanism for membranes, we must recognize that some regions of the membrane may undergo stretching up to a point where the membrane reservoirs are fully exhausted. For the thin fibers composing the membrane, pure stretching deformations represent a far higher energetical cost relative to bending deformations (*23*), and as a first approximation, this sharp energetical penalty can be seen as an inextensibility constraint. The shapes adopted by the planar configuration can therefore be captured with a surface area minimization under isoperimetric constraint (*16*) (figs. S11 to S13). This mixed liquid-solid behavior allows stabilization of the catenoid shape beyond its classic point of bursting to unveil new equilibria (*16*) (Fig. 3, D to F, and figs. S14 and S15), and is also responsible for considerable deviations from Laplace's law in the bubble configuration (Fig. 3, G to I). Such a hybrid mechanical behavior is again reminiscent of the response of cellular membranes, and indeed, whether for lymphocytes, fibroblasts (*3*, *6*), or wicked membranes (Fig. 3), the mechanical response switches from liquid-like to solid-like once all the membrane reservoirs have been smoothed out.

The peculiar behavior of our wicked membrane stems from its compound nature: Capillarity-induced folds allow it to undergo ample shape changes while remaining taut, while its solid underlying matrix provides mechanical robustness. Geometrical reorganizations at the microstructural level (reservoir folding or unfolding) are key in the mechanics of the wicked membrane, and in particular they prevent any notable

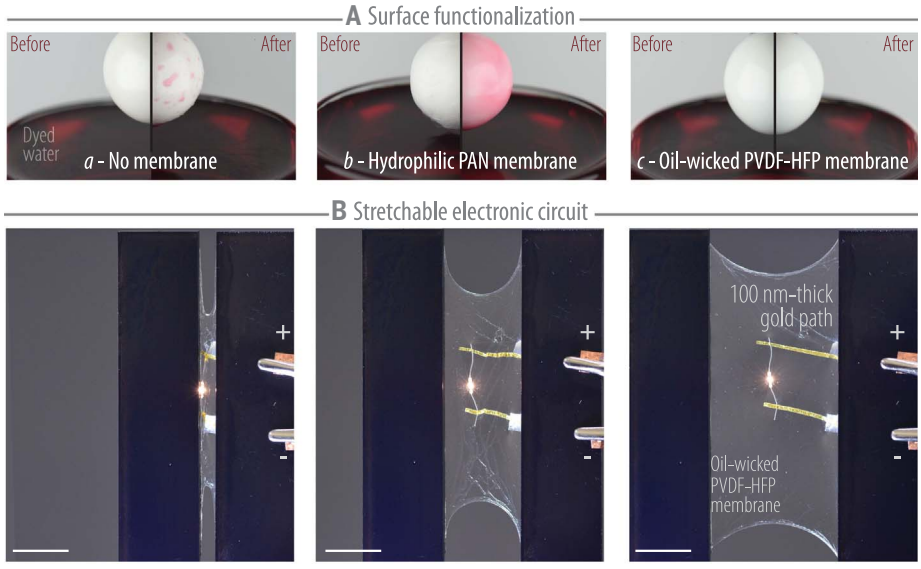

Fig. 4. Conformability and stretchability for chemical and electrical functionalization of the wicked membrane. (**A**) Without previous treatment (a), a clean zircon bead is dipped in a dyed water bath and subsequently pulled out. A water film is drawn at the bead surface, and because water only partially wets zircon, it rapidly disintegrates into droplets. A dry hydrophilic PAN membrane (b) is now applied on the bead and the experiment is repeated. After dipping and extracting the bead around 10 times, water has percolated through the membrane, and the bead is coated with a fairly homogeneous dyed water film, the PAN membrane adapts to the bead surface and secures the water film, thus providing a hydrophilic surface treatment. The bead is now covered with a silicone oil–wicked PVDF-HFP membrane (c), which acts as a water repellent coating; when the bead is dipped and pulled out of the bath, no water is drawn at its surface. Diameter of the zircon bead: 1.5 cm. (**B**) Two 100-nm-thick gold strips are affixed to a silicone oil–wicked PVDF-HFP membrane and are connected to a 1.55-V LED. Capillary adhesion secures the gold paths to the membrane and in the compressed state, they follow the folding of membrane reservoirs. Electricity runs through this elementary circuit when membrane reservoirs are smoothed out upon the reversible factor of 8 extension. Scale bar, 1 cm.

stretching at the molecular level. This results in a marked resistance of this material to fatigue, as illustrated by the unvarying mechanical response of the membrane after more than 100,000 cycles of extension and compression by a factor of 10 (*16*) (Fig. 3C and figs. S3 and S4).

The mechanics of reservoir folding and unfolding is a priori material-independent, as it relies only on a combination of elasticity, capillarity, and geometry (see tested polymers in table S1). To illustrate a few potential applications, we present some proofs of concept in Fig. 4. First, we demonstrate how the natural conformability of the wicked membrane can be used to confer instant chemical functions to nonplanar surfaces. As an example, we tune the chemical surface properties of a zircon bead. At its native state, the bead is dipped and pulled out from a dyed-water bath, thus withdrawing a liquid film. Zircon is only partially wet by water, and the liquid film coating the bead therefore rapidly disintegrates into a series of droplets (Fig. 4A, panel a, and movie S6). We now cover the bead with a hydrophilic (PAN) membrane and repeat the experiment. As soon as the bead is pulled out from the bath, the membrane folds within the drawn liquid film and therefore adapts to the bead curvature (Fig. 4A, panel b, and movie S7). Here, the membrane acts as an adaptable scaffold that secures and stabilizes the liquid film onto the bead. Conversely, this strategy can also be used to prevent contact between the bead and water: If the bead is covered with a silicone oil–wicked oleophilic membrane (a PVDF-HFP membrane), its surface inherits both the immiscible character and low surface energy of oil. After the bead is withdrawn from the bath, no water trace remains at the bead surface (Fig. 4A, panel c, and movies S8 and S9). We now show how stretchability can be combined with electrical function (fig. S7). In Fig. 4B, we affix 100-nm-thick gold paths to a wicked PVDF-HFP membrane to design an elementary electronic circuit. A LED is powered through the metallic tracks that follow the deformation of the membrane. When the membrane is compressed, the tracks are localized in the membrane reservoirs. Upon extension, these tracks are unfolded, thus exhibiting conductivity throughout a factor of 8 extension-compression cycle (*16*) (Fig. 4B and movie S10).

The use of membrane reservoirs to fuel large shape changes is encountered in a variety of animal cells. Our results show that capillarity-induced folding in thin wicked membranes endows conventional materials with large effective stretchability and conformability, and thereby constitutes a promising tool for the design of soft deformable materials.

REFERENCES AND NOTES

1. H. Elettro, S. Neukirch, F. Vollrath, A. Antkowiak, *Proc. Natl. Acad. Sci. U.S.A.* **113**, 6143–6147 (2016).
2. J. Lam, M. Herant, M. Dembo, V. Heinrich, *Biophys. J.* **96**, 248–254 (2009).
3. L. Guillou *et al.*, *Mol. Biol. Cell* **27**, 3574–3582 (2016).
4. D. Raucher, M. P. Sheetz, *Biophys. J.* **77**, 1992–2002 (1999).
5. J. Dai, M. P. Sheetz, *Biophys. J.* **68**, 988–996 (1995).
6. N. Groulx, F. Boudreault, S. N. Orlov, R. Grygorczyk, *J. Membr. Biol.* **214**, 43–56 (2006).
7. J. A. Nichol, O. F. Hutter, *J. Physiol.* **493**, 187–198 (1996).
8. C. A. Erickson, J. P. Trinkaus, *Exp. Cell Res.* **99**, 375–384 (1976).
9. S. Majstoravich *et al.*, *Blood* **104**, 1396–1403 (2004).
10. G. Salbreux, G. Charras, E. Paluch, *Trends Cell Biol.* **22**, 536–545 (2012).
11. J. A. Rogers, T. Someya, Y. Huang, *Science* **327**, 1603–1607 (2010).
12. W. Liu, M.-S. Song, B. Kong, Y. Cui, *Adv. Mater.* **29**, 1603436 (2017).
13. J. Hu, H. Meng, G. Li, S. I. Ibekwe, *Smart Mater. Struct.* **21**, 053001 (2012).
14. R. F. Shepherd *et al.*, *Proc. Natl. Acad. Sci. U.S.A.* **108**, 20400–20403 (2011).
15. A. Lazarus, P. M. Reis, *Adv. Eng. Mater.* **17**, 815–820 (2015).
16. See supplementary materials.
17. E. Cerda, L. Mahadevan, *Phys. Rev. Lett.* **90**, 074302 (2003).
18. T. Tallinen *et al.*, *Nat. Phys.* **12**, 588–593 (2016).
19. H. Vandeparre *et al.*, *Phys. Rev. Lett.* **106**, 224301 (2011).
20. B. Davidovitch, R. D. Schroll, D. Vella, M. Adda-Bedia, E. A. Cerda, *Proc. Natl. Acad. Sci. U.S.A.* **108**, 18227–18232 (2011).
21. B. Roman, J. Bico, *J. Phys. Condens. Matter* **22**, 493101 (2010).
22. B. Roman, A. Pocheau, *Europhys. Lett.* **46**, 602–608 (1999).
23. B. Audoly, Y. Pomeau, *Elasticity and Geometry: From Hair Curls to the Nonlinear Response of Shells* (Oxford Univ. Press, 2010).

ACKNOWLEDGMENTS

We thank I. Genois for SEM pictures, F. Poydenot for electrical resistance characterization, and T. Bastien for the fabrication of the fatigue test setup. **Funding:** Supported by ANR grant ANR-14-CE07-0023-01 and by CNRS PEPS-PTI and PICS grants. **Author contributions:** P.G., A.A., and S.N. designed the study; N.K. and C.L.-R. designed the electrospinning setup; N.K. and P.G. fabricated the membranes; P.G. and A.H.-F. performed the experiments and acquired the data; A.A., P.G., A.H.-F., and S.N. interpreted the data and proposed the mechanical models; and A.A. and P.G. wrote an initial version of the manuscript and all authors reviewed it. **Competing interests:** None. **Data and materials availability:** All data are available in the manuscript or the supplementary materials. **Patent:** P.G., A.A., N.K., and C.L.-R. are inventors on French patent application FR 1751950 submitted by Sorbonne Université on "composite membrane and manufacturing process of such a membrane."

SUPPLEMENTARY MATERIALS

www.sciencemag.org/content/360/6386/296/suppl/DC1
Materials and Methods
Supplementary Text
Table S1
Figs. S1 to S20
Movies S1 to S10
Data Files
References (*24–26*)

27 September 2017; accepted 22 February 2018
10.1126/science.aaq0677

Science

Capillarity-induced folds fuel extreme shape changes in thin wicked membranes

Paul Grandgeorge, Natacha Krins, Aurélie Hourlier-Fargette, Christel Laberty-Robert, Sébastien Neukirch and Arnaud Antkowiak

Science **360** (6386), 296-299.
DOI: 10.1126/science.aaq0677

Reserving the right to stretch

Retractable antennae or certain spider silks can stretch well beyond their apparent length because they have a reserve of material that lets them expand and contract over much longer distances. Grandgeorge *et al.* made nonwoven fibrous membranes by electrospinning a block copolymer with varying ratios of two components. They infused these membranes with a liquid that let the fibers buckle and fold without changing the apparent surface area. When the membranes were stretched, this material could unbuckle and slide along the membrane surface, allowing it to extend without breakage.

Science, this issue p. 296